THE MODEL MEMBRANE SYSTEM

EGG LECITHIN + MYELIN PROTEIN (N-2).

EFFECT OF SOLVENT DENSITY VARIATION ON THE X-RAY SCATTERING

G. W. BRADY AND P. S. BIRNBAUM, *Division of Laboratories and Research, New York State Department of Health, Albany, New York 12201 and Center for Biological Macromolecules, State University of New York, Albany, New York 12222 U.S.A.*

M. A. MOSCARELLO, *Department of Biochemistry, Research Institute, Sick Children's Hospital, Toronto, Ontario, Canada*

ABSTRACT The electron density contrast method has been applied to the membrane system egg lecithin + myelin protein (N-2). The case treated here is for a low protein concentration. As theory predicts, the scattering from the different regions of the membrane (protein, hydrocarbon, and polar head group regions) are modulated differently by changing the contrast. It is then possible to separate out the electron pair correlation functions for the different regions, and from these to determine the membrane election density distribution for an external electron density $\rho_0 = 0$.

INTRODUCTION

We present in this paper the results of a study of the effect of the variation of the solvent electron density, ρ_0, on the scattering from the model membrane system (N-2) myelin protein + egg lecithin. This method is actually a modification of the technique, widely used in crystallographic studies, of enhancing a structural feature by incorporating high scattering atoms at specified locations in the crystal. The incorporation procedure has also been extended successfully to noncrystalline systems by Kratky (1947, 1948) in studies on dissolved molecules, by Brady in studies on polystyrene (1964), the α-helix (1965) and liquid alkanes (1974), and by Schmatz (1974) and Wignall (1974) in neutron studies on polymers (this cited work is representative, not inclusive). In large biological molecules or aggregates, which have extended regions of constant electron density, ρ_i, occupying the whole or part of the aggregate or molecular volume, the enhancement can often be more conveniently done by lowering or raising the electron density of the solvent in which the sample is immersed; the scattered intensity then is proportional to $(\rho_i - \rho_0)^2$. Bragg and Perutz (1952) did studies on the external form of hemoglobin by varying the salt concentration of the surrounding medium. A descriptive article on the use of H_2O-D_2O mixtures as solvent in neutron small-angle scattering has been presented by Stuhrmann (1974). Schoenborn (1976) has discussed

---

This paper was part of the Symposium on Interactions between Membrane Components, organized by Stephen H. White, held at the Annual Meeting of the Biophysical Society on 26 March 1978.

the application of the D_2O-H_2O technique more specifically to membranes. The work of Moore et al. (1977) on ribosomes is an elegant example of the method's capability.

With respect to X-rays, work on low density lipoprotein by Mateu and co-workers (1972) and by Laggner et al. (1974) using this technique has been of interest in showing how the electron density fluctuations in spherically symmetrical particles can be characterized. Earlier work by Worthington and Blaurock (1969) on nerve myelin membrane was particularly relevant in showing how the constant modulation experiments (in sucrose or glycerol solutions) could be used to determine absolute electron densities and the phases of higher-order reflections.

Previous work on the present system (Brady et al., 1979) had shown that the protein was located at the center of the bilayer, and existed as a spherical particle with a radius of 54 Å. The contrast variation method should provide further evidence for this configuration, and, as will be discussed presently, should permit a separation of the contributions to the scattering of the hydrocarbon and polar regions of the phospholipid bilayer. The results presented here were obtained on a system at 4% protein concentration. The previous study had shown that the contributions of the lipid-protein pair correlation terms (to be later identified as D_{12} and D_{13}) were small at protein contributions less than 6%. Minimizing these terms leads to a useful simplification in the calculations. A forthcoming publication will treat the high protein (35%) case.

THEORY

For a membrane consisting of three different electron density regions ρ_i (protein), ρ_2 (hydrocarbon), and ρ_3 (polar head group region), suspended in a medium of electron density ρ_0, the scattered intensity is given by the expression

$$I(s) = \int_0^\infty \sum_{i,j=1}^{3} \bar{v}_i, \bar{v}_j(\rho_i - \rho_0)(\rho_j - \rho_0)C_{ij}(r)(\sin sr/sr)4\pi r^2 \, dr, \tag{1}$$

where $\bar{v}_i$, $\bar{v}_j$ are volume fractions, $C_{ij}(r)$ is an electron pair correlation function and $s = 4\pi/\lambda \sin \Theta$; $\lambda = 1.54$ Å is the radiation wavelength and Θ is one-half the scattering angle. Its Fourier transform is

$$r \sum_{i \geq j=1}^{3} D_{ij}(r) = (1/2\pi^2) \int_0^\infty sI(s) \sin rs \, ds, \tag{2}$$

where

$$D_{ij}(r) = \bar{v}_i\bar{v}_j(\rho_i - \rho_0)(\rho_j - \rho_0)C_{ij}(r). \tag{3}$$

Since, relative to an aqueous buffered solvent, $(\rho_i - \rho_0)$ and $(\rho_3 - \rho_0)$ are positive and $(\rho_2 - \rho_0)$ is negative, raising the solvent density will decrease the contributions of the protein and polar regions and increase the contribution of the hydrocarbon region. This enables identification of the individual D_{ij} terms. In fact, if the individual terms of Eq. 2 (or Eq. 1) are written down, we have for the $i = j$ terms: $D_{11}(r) = \bar{v}_1^2(\rho_1 - \rho_0)^2C_{11}(r)$, with similar terms for $D_{22}(r)$ and $D_{33}(r)$. For the $i \neq j$ terms we have $D_{13}(r) = \bar{v}_1\bar{v}_3(\rho_1 - \rho_0)(\rho_3 - \rho_0)$ $C_{13}(r)$, with similar terms for D_{12} and D_{23}. It is evident that if $D_{ij}(r)$ is determined at six

different values of ρ_0, a set of six linear equations with independent coefficients results, and consequently the six C_{ij}'s can be determined by solving the appropriate determinants. The same procedure can be used with the intensity equations, where the separate contributions of the six integrals to the total intensity can be evaluated. The advantage of this procedure is that the lipid and protein terms can be separated and grouped together in the appropriate way and their electron density distribution evaluated. Thus, $D_{lip} = D_{22} + D_{33} + D_{23}$; $D_{prot} = D_{11}$. The D_{12} and D_{13} terms come from the correlations between the electrons of the protein and lipid and can be used to locate the position of the protein in the membrane.

This method is applicable to both neutrons and X-rays; the former technique has the great advantage that the contrast can be varied over a much wider range by taking advantage of the great difference in scattering length between D_{20} and H_2O. With X-rays, one is limited in the choice of solvents; the two most commonly used are sucrose and glycerol solutions. Luzzati (1972) has successfully used NaBr, but here a correction is needed for the partition of the added ions between the solvent and the polar regions of the membrane. Nevertheless, the range over which ρ_0 can be varied is adequate for our purposes. The intensity patterns must be determined accurately, however.

A complicating factor in the analysis is the swelling of the membrane in the different solvents. Blaurock (1971) had noted this in studies of frog sciatic nerve myelin in solutions of different sucrose concentrations. His analysis showed that the bilayer structure was not affected, but that there was a significant effect on the interbilayer structure, as manifested by an increase in the interbilayer distance, and a broadening and/or change in the multilayer peak areas. In the present system (at low protein concentration), there is considerable multilayer structure present, and we find that its contribution to the total scattering behaved in an analogous manner with respect to the solvent. Since the method is strictly valid only for cases where the solvent affects only the contrast, the multilayer contribution had to be identified and removed from the intensity pattern before we proceeded with the analysis.

METHODS

X-Ray Measurements and Data Processing

The patterns were measured and corrected for absorption and background as previously described (Brady et al., 1969). A Kratky apparatus was used and the data was collected, stored, and least-squares averaged in a PDP8/E minicomputer (Digital Equipment Corp., Maynard, Mass.); the error per point was less than 1%. The Schmidt program (Schmidt and Hight, 1960) was used for desmearing. Fourier transforms, deconvolutions, and other data manipulations were done directly in the PDP8/E. The Pape (Pape, 1974) deconvolution procedure was used. The data could be read out on a teletype or displayed on an oscilloscope at any stage of the processing.

Materials

The procedure and characterization of the samples has been previously described (Brady et al., 1979). Hydrophobic myelin protein (N-2) was incorporated into egg lecithin by the method of Boggs et al. (1976), with minor modifications. The egg lecithin was dissolved in a small volume of 100% 2-chloroethanol (2 mg lipid/0.4 ml solvent). The dry protein was dissolved in 100% 2-chloroethanol at a concentration of 5 mg/ml and sonicated briefly with a probe sonicator. The two solutions were combined in the desired ratio (protein:lipid = 5:100) and the resultant suspension was separated into six aliquots. These were dialyzed against 4 liters of N-2-hydroxyethylpiperazine-*N'*-2-ethanic sulfonic acid (HEPES) buffer (10 mM Na^+, 2 mM HEPES, 0.1 mM EDTA), pH 7.4. The dialysis bath was changed once.

The samples were then made to varying concentrations of sucrose by dialyzing against 2 liters of HEPES containing 10, 20, 30, 40, and 50% sucrose, respectively. The sixth sample was dialyzed against 2 liters of HEPES without sucrose. The corresponding electron densities in electrons/Å^3 were, for the six solutions: 0%, 0.334; 10%, 0.345; 20%, 0.354; 30%, 0.363; 40%, 0.370; 50%, 0.377; the suspensions were concentrated before use by centrifuging. The final concentrations were in the range 30–40 mg/ml of suspended material. The resultant scattering curves were normalized to the concentration of the 0% sucrose sample. The samples were analyzed for total weights of suspension, and for percent protein and phospholipid by amino acid analysis on a Technicon TSM amino acid analyzer (Technicon Instruments Corp., Tarrytown, N.Y.) and by phosphorus assay according to a modified Bartlett (1959) procedure.

The values used for the electron densities of protein (ρ_1), hydrocarbon region (ρ_2), and polar head group region (ρ_3) were 0.355, 0.270, and 0.380 electrons/Å^3, respectively.

RESULTS AND DISCUSSION

The desmeared curves are shown in Fig. 1; the ρ_0 values appropriate to each curve are listed. Qualitative features to note are the scattering at the smallest angles to the left of $s \simeq 0.09$, and the large peak, almost a reflection at $s \simeq 0.10$. This latter corresponds to a real space distance of ~74 Å and is thus identified with a multilayer structure component. This peak shifts to smaller angle with increasing ρ_0, and first broadens, with an apparent decrease in area, and then increases in intensity. The smaller-angle intensity also decreases at first and then increases. Such a behavior agrees qualitatively with the equations, which show that simultaneous increases and decreases of the different scattering components should occur. A further feature of the curves is the gradual increase and extension of the small-angle component of the scattering out to $s \simeq 0.19$. This manifests itself as an increasing background on which the multilayer peak sits.

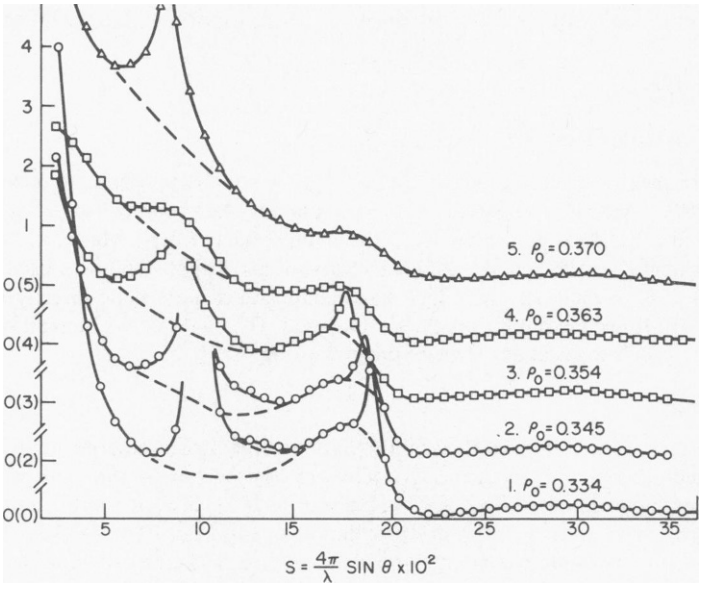

FIGURE 1 Membrane intensity patterns measured at the five different values of the solvent electron density listed in each curve.

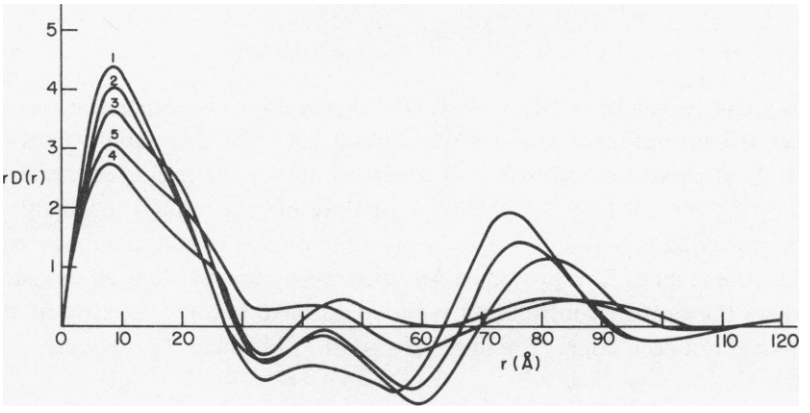

FIGURE 2 Fourier transforms of the curves of Fig. 1.

Fig. 2 shows the Fourier transforms of Fig. 1. Removing the multilayer features before transforming results in Fig. 3 (see caption). The curves in Fig. 3 are characterized by a maximum at ~44 Å, preceded by a negative minimum; these two features decrease as ρ_0 increases. A second feature is the presence of a shoulder with an apparent maximum at $r \simeq 17$, which increases steadily with increasing ρ_0. The first of these components is identified with the phospholipid contribution (Brady et al., 1979). The second will be discussed later. Not visually evident in Fig. 3, but present, is a broad band extending out to ~108 Å, on which these features are superimposed. To bring it into evidence and to identify it with the protein contribution, we show in Fig. 4 the small angle region of Fig. 1, plotted on an expanded scale. The protein contribution to the small-angle scattering (as well as its transform) has been identified (Brady et al, 1979) and indicates that the protein is present as a spherical particle of radius 54 Å. The scattering curve for a spherical particle of this radius, calculated from the Rayleigh equation

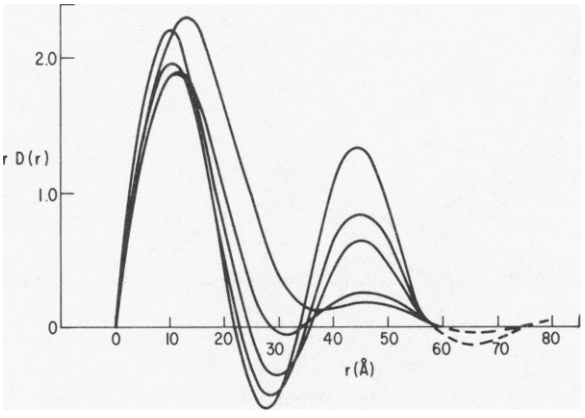

FIGURE 3 Fourier transforms of the curves of Fig. 1 after removal of the multilayer features; these are the peak at $s \simeq 0.09$ and $s \simeq 0.19$. The peaks at $s \simeq 0.19$ are only evident in the first three curves. Both sets of peaks move to smaller angle with increasing ρ_0.

$$I_s = \nu^2\rho^2\phi^2(sR) = K\frac{9\pi}{2}\left[\frac{J_{3/2}(sR)^2}{(sR)^{3/2}}\right], \tag{4}$$

where K is a scaling constant and R = 54 Å, is also plotted. The expression was averaged over a Gaussian distribution of radii between $R \pm 0.1\,R$. The calculated values from Eq. 4 scaled to those of curve 1 are shown as filled circles. Since the measured curve shows significant scattering at $s = 0.07$, where the calculated protein scattering is negligible, the curve through the scattering at $s = 0.07$ was extrapolated into $s = 0.05$ and subtracted from the total curve before scaling. This procedure was dictated by the fact that all the curves except curve 4, where the protein contribution is 0, would have become negative at the smaller angles if this had not been done. The fit is very good. This intensity obviously corresponds to the term in Eq 1: $I = (\rho_1 - \rho_0)^2\bar{v}_1^2\int_0^\infty 4\pi r^2 C_{11}(\sin sr/sr)\,dr$; $I = (\rho_1 - \rho_0)^2\,\bar{v}_1^2\phi^2(sR)$, with $i = j = 1$. The protein contributions can then be evaluated for each solvent electron density by multiplying by the appropriate factor $(\rho_1 - \rho_0)^2$. These are also shown on the figure as open circles. When subtracted from the total measured intensity, the presence of the other small-angle component is made much more evident. It can now be seen to have a negative slope at the lower angles. (There is evidence of a slight maximum at $s \simeq 0.13$, which could be due to the presence of a small amount of lipid-protein scattering. It makes a minor contribution to a total and will not be discussed further.) The outer boundary of the small-angle scattering is completed by extrapolating the curve to 0 at $s \simeq 0.19$. This is done to fix an upper limit for the small-angle scattering so that its Fourier transform can be isolated. In

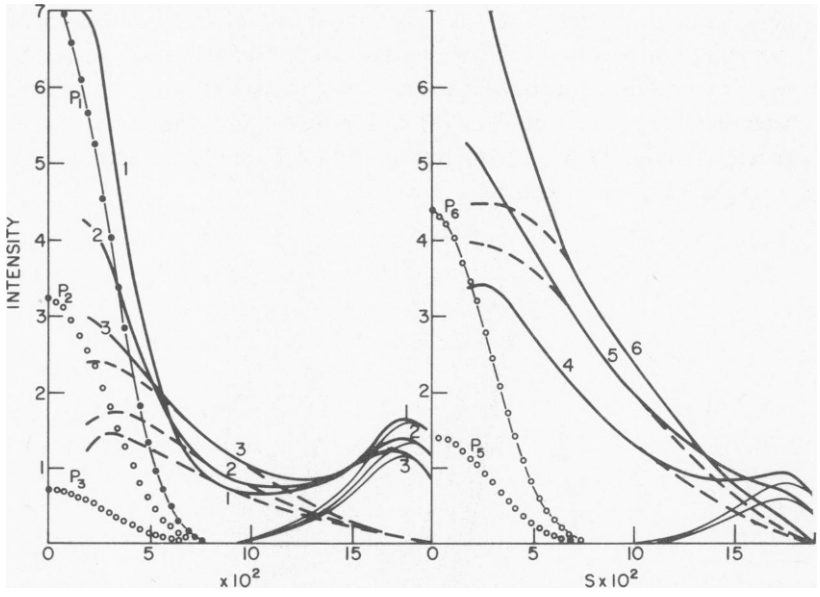

FIGURE 4 The intensity patterns at the smaller angles plotted in an expanded abscissa scale. Curve 6 is for $\rho_0 = 0.371$. The closed circles represent the calculated scattering curve of a spherical protein particle of 54 Å radius, normalized to the measured curves for $\rho_0 = 0.334$ (curve P_1). The open circles are this curve, scaled by the factor $(\rho_1 - \rho_0)^2$ (curves $P_2 - P_6$). The dashed portion of the curves is the difference between the measured curve and the scaled protein curves (see text). The left-hand side of the peak at $s \simeq 0.19$ has been sketched in (see text).

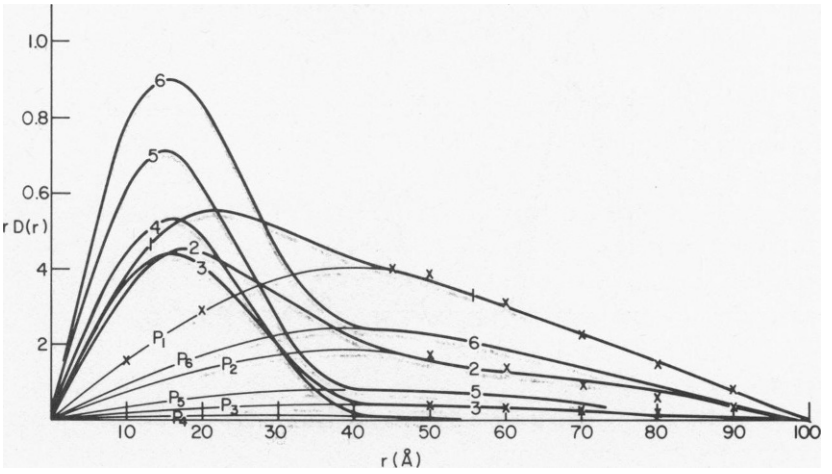

FIGURE 5 Fourier transforms of the scattering curves at smaller angles (Fig. 4). The presence of two different pair correlations is clearly evident. The crosses are the transforms calculated from Eq. 5.

the later analysis, the total curve will again be used, so no arbitariness is introduced by this procedure. The transforms are shown in Fig. 5.

Inspection of Fig. 5 shows even more clearly the existence of the two separate components of the small-angle scattering. We again identify the protein with the broad component extending out to $\sim 10^8$ Å and exhibiting a maximum at ~ 40 Å. This is confirmed by calculating the Fourier transform of the scattering of a spherical particle from the equation

$$rD(r) = r\{1 - (3/4)(r/R) + \frac{1}{16}[(r/R)]^3 - \ldots\}, \tag{5}$$

again with $R = 54$. These are plotted as crosses in the figure. The agreement with the experimental curves beyond $r \simeq 40$ is also very good. The other component is then isolated, as shown in the figure. This latter, after passing through the maximum at 17–18 Å, tails off to 0 at $r \simeq 39$–41 Å. Its magnitude increases with increasing ρ_0. Since the only term in Eq. 2 that increases with ρ_0 is that due to the hydrocarbon, we associate this correlation with the negative electron density at the interior of the bilayer. In fact, the intensity at the maximum does increase approximately as $(\rho_2 - \rho_0)^2$; thus this feature is identified wholly or in large part with the $rD_{22}(r)$ term. As such, it is to be included in the total phospholipid transforms $R(D_{22} + D_{33} + D_{23})$. These are evidently the curves of Fig. 3 with the protein contribution (from Fig. 5) subtracted, and are displayed in Fig. 6.

Because the curves of Fig. 6 are free of the protein contribution D_{11} and the lipid-protein correlation terms D_{12} and D_{13}, the analysis is simplified considerably, since it reduces the analysis to the solution of three simultaneous equations, which can be obtained by solving for a third-order instead of a sixth-order determinant. Dividing by r we have

$$[D_{\text{lip}}(r)]\rho_0 =$$

$$\bar{v}_2^2(\rho_2 - \rho_0)^2 C_{22}(r) + \bar{v}_3^2(\rho_3 - \rho_0)C_{33}(r) + 2\bar{v}_2\bar{v}_3(\rho_2 - \rho_0)(\rho_3 - \rho_0)C_{23}(r), \tag{6}$$

where each curve of Fig. 7 represents $D(r)$ for a different value of ρ_0. The coefficient of C_{23}

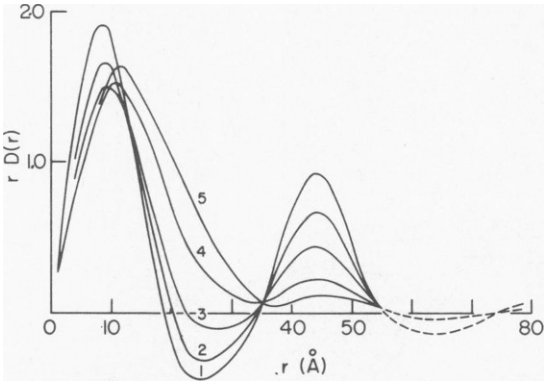

FIGURE 6 Fourier transforms with the protein contribution removed.

is negative. Dividing by $\bar{v}_2^2$, we get $(1/v_2^2)[D_{\text{lip}}(r)]\rho_0 = (\rho_2 - \rho_0)^2 C_{22}(r) + \alpha^2(\rho_3 - \rho_0)^2 C_{33}(r) + 2\alpha(\rho_2 - \rho_0)(\rho_3 - \rho_0)C_{23}(r)$, where $\alpha = (\bar{v}_3/\bar{v}_2)$ is the ratio of the volumes of polar group to hydrocarbon regions. This ratio depends on the composition of the phospholipid present. We chose a value of 0.59, the ratio of the total thickness of polar group to hydrocarbon regions in egg lecithin (Brady et al., 1979). Obviously the ratio will not affect the physics of the situation, but will change the relative contributions of the ρ_2 and ρ_3 terms. Inserting the appropriate values for the ρ's and combining the various constants and scaling factors into a single constant β, we have $\beta[D(r)]_{\rho_0 = 0.334} = 11.85\ C_{22} + 2.116\ C_{33} - 9.996\ C_{23}$; $\beta[D(r)]_{\rho_0 = 0.345} = 14.56\ C_{22} + 1.520\ C_{33} - 9.384\ C_{23}$; $\beta[D(r)]_{\rho_0 = 0.354} = 17.77\ C_{22} + 0.999\ C_{33} - 8.398\ C_{23}$, with equivalent equations for the other three values of ρ_0. Any three of the six equations can be used. The determinant solution is sensitive to error in the relative value of $[D(r)]_{\rho_0}$, particularly near the points where the function is zero, so the correlation functions were calculated for all possible combinations of sets of three of the curves in

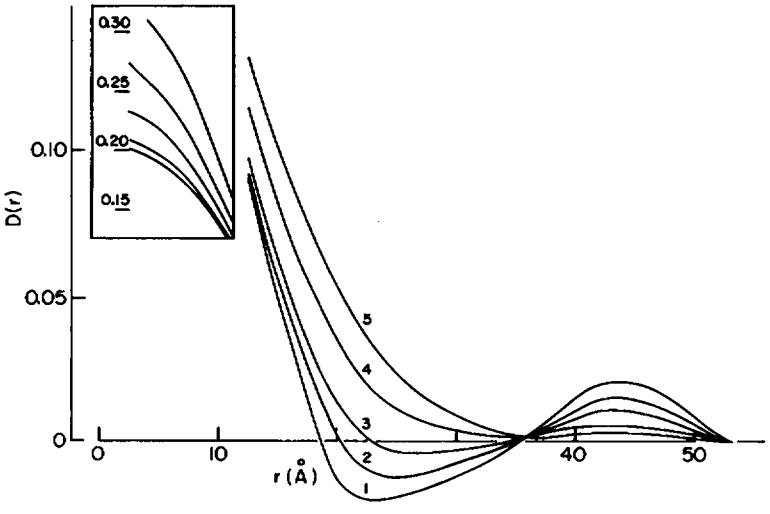

FIGURE 7 Fig. 6 divided by r.

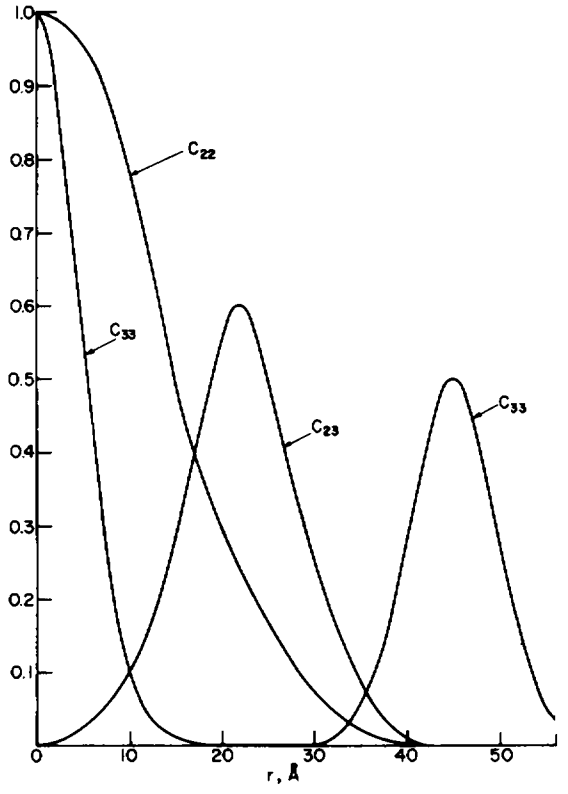

FIGURE 8 The isolated electron pair correlation functions C_{22}, C_{33}, and C_{23}.

Fig. 7, and the results meaned. Where necessary, adjustments of $\pm 10\%$ were made in some of the points so that a consistent set of values for all the combinations was obtained. The three resolved correlation functions are shown in Fig. 8.

The analysis of the data by this method offers positive advantages. It gives a clear meaning to the C_{22}, C_{33}, and C_{23} functions and shows how they relate to the scattering of the individual terms. Thus both C_{22} and C_{33} should be unity at $r = 0$. The range of C_{22} will be over a distance equal to the width of the interior hydrocarbon region of the bilayer. It will decrease to zero over this range. The C_{33} term will first decrease to zero as r approaches a value comparable to the head group thickness, and then rise to a maximum again as the electron density in the polar region on one side of the membrane correlates with that region on the other side. It then falls to zero at the bilayer boundary. C_{23} will be zero when $r = 0$ and when r approaches a distance equal to the sum of the widths of the hydrocarbon and polar regions, being finite and positive between these boundaries. As Fig. 7 shows, the three functions possess these features. A further advantage of this technique is that the C's can now be used to evaluate the transforms (or the intensity patterns) at any value of ρ_0, including $\rho_0 = 0$; thus the electron pair distributions in the absence of solvent can be evaluated.

The electron density distribution through the membrane can then be obtained by a deconvolution. It should be noted that the C_{23} term measures only those distances where an

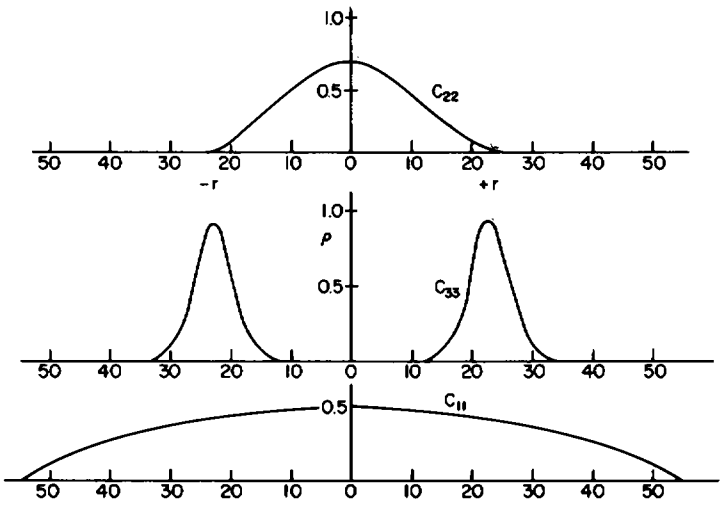

FIGURE 9 The deconvoluted functions C_{22}, C_{33}, and C_{11}.

electron density ρ_2 is correlated with an electron density ρ_3; it thus makes explicit how the structures characterized by C_{22} (the hydrocarbon region) and C_{33} (the polar head group region) are spatially fixed relative to each other. The form of C_{23} indicates that C_{22} and C_{33} are symmetrically placed about a common origin, the bilayer center, and thus the phospholipid electron density will be given by the sum of the deconvoluted values of D_{22} and D_{33}, that is the sum of the deconvoluted C_{22} and C_{33}, each multiplied by its appropriate electron density. Similarly, the total membrane density profile will be given by the sum of the deconvoluted values of C_{11}, C_{22}, and C_{33} multiplied by their electron densities, since the C_{12} and C_{13} terms in turn measure only how C_{11} is fixed relative to C_{22} and C_{33}. As noted, the C_{12} and C_{13} terms were suppressed by keeping the protein concentration low. However, our previous semiquantitative evaluation of these quantities, or more specifically $D_{12} + D_{13}$ (Brady et al., 1979), indicated that the protein was also symmetrically placed about the origin. The deconvoluted curves for C_{11}, C_{22}, and C_{33} are shown in Fig. 9. In Fig. 10, the sum $D_{11} + D_{22} + D_{33}$ for $\rho_0 = 0$ is shown. This is, finally, the bilayer profile. Note that it differs from its value in absolute units by the scaling constant β.

In a succeeding publication we will discuss the application of this method to this same

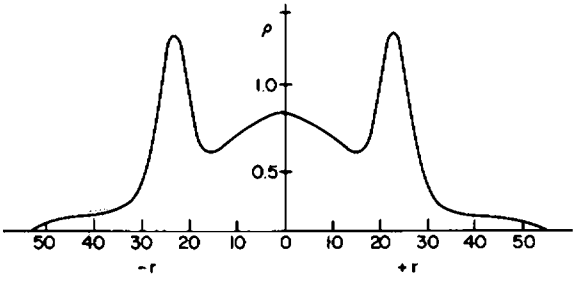

FIGURE 10 The membrane profile at $\rho_0 = 0$.

system at high protein (35%) concentration, where the D_{12} and D_{13} contributions will be significant. When this is done, a complete characterization of the six correlation terms will have been achieved.

We would like to acknowledge the assistance of N. S. Murthy in most of the calculations.
This work was supported by a grant, PCM76-07569, from the National Science Foundation.

Received for publication 31 July 1978 and in revised form 22 November 1978.

REFERENCES

BARTLETT, G. R. 1959. Colorimetric assay for free and phosphorylated glyceric acids. *J. Biol. Chem.* **234**:469–471.

BLAUROCK, A. E. 1971. Structure of nerve myelin membrane: proof of the low resolution profile. *J. Mol. Biol.* **56**: 35–52.

BOGGS, J. M., W. J. VAIL, and M. A. MOSCARELLO. 1976. Preparation and properties of vesicles of a purified myelin hydrophobic protein and phospholipid. A spin label study. *Biochim. Biophys. Acta.* **448**:517–530.

BRADY, G. W. 1974. On the aggregation of dissolved alkane chain molecules. *Acc. Chem. Res.* **7**:174–180.

BRADY, G. W., P. S. BIRNBAUM, M. A. MOSCARELLO, and D. PAPAHADJOPOULOS. 1979. Liquid diffraction analysis of the model membrane system. Egg lecithin + myelin protrom (N-2). *Biophys. J.* **26**:23–42.

BRADY, G. W., C. COHEN-ADDAD, and E. F. X. LYDEN. 1969. Structure studies of solutions of large organic molecules. I. $C_8H_{19}I$ and $C_{18}H_{36}I_2$ in decalin. *J. Chem. Phys.* **51**:4309–4319.

BRADY, G. W., and R. SALOVEY. 1964. X-ray diffraction studies of the conformation of polymer molecules in solution. I. *p*-Iodopolystyrene. *J. Am. Chem. Soc.* **86**:3499–3503.

BRADY, G. W., R. SALOVEY, and J. M. REDDY. 1965. X-ray diffraction studies of the conformation of polymer molecules in solution. II. poly-3,5-dibromotyrosine. *Biopolymers.* **3**:573–583.

BRAGG, L. W., and M. F. PERUTZ. 1952. The external form of the hemoglobin molecule. *Acta. Crystallogr. Sect. B Struct. Crystallagr. Cryst. Chem.* **5**:277–283.

KRATKY, O., G. POROD, and A. SEKORA. 1948. Zur roentgenographischen untersuchung vernauelung gelöster faden molekules. *Monatsh. Chem.* **78**:295–296.

KRATKY, O., and W. Worthman. 1947. Über die Bestimmbarkeit der konfiguration geloster organisder molekülе durch interferometrische vermessungmit Roentgenstrahlen. *Monatsh. Chem.* **76**:263–281.

LAGGNER, P., K. MULLER, and O. KRATKY. 1974. X-ray small angle scattering of human serum lipoproteins. *J. Appl. Crystallogr.* **7**:179–183.

MATEU, L., A. TARDIEU, V. LUZZATI, L. AGGERBECK, and A. M. SCANU. 1972. On the structure of human serum low-density lipoprotein. *J. Mol. Biol.* **70**:105–116.

MOORE, P. B., J. A. LANGER, B. P. SCHOENBORN, and O. M. ENGELMAN. 1977. Triangulation of proteins in the 30s ribosomal subunit of *Escherichia coli*. *J. Mol. Biol.* **112**:199–234.

PAPE, E. H. 1974. A new deconvolution method for evaluating electron density distributions from small angle X-ray scattering diagrams. *Biophys. J.* **14**:284–292.

SCHMATZ, W., T. SPRINGER, J. SCHELTEN, and K. IBEL. 1974. Neutron small angle scattering. Experimental techniques and application. *J. Appl. Cryst.* 7:96–105.

SCHMIDT, P. W., and J. HIGHT. 1960. Slit height corrections in small angle X-ray scattering. *Acta. Crystallogr. Sect. B Struct. Crystallogr. Cryst. Chem.* **13**:480–496.

SCHOENBORN, B. P. 1976. Neutron scattering for analysis of membranes. *Biochim. Biophys. Acta.* **457**:41–55.

STUHRMANN, H. 1974. Neutron small angle scattering of biological macromolecules in solution. *J. App. Crystallogr.* **7**:173–178.

WIGNALL, G. D., J. SCHELTEN, and D. G. H. BALLARD. 1974. Measurements of radius of gyration and persistence length in bulk atactic polystyrene by low angle neutron scattering. *J. Appl. Crystallogr.* **7**:190–196.

WORTHINGTON, C. R., and A. E. BLAUROCK. 1969. A low angle x-ray diffraction study of swelling behavior of peripheral nerve myelin. *Biochim. Biophys. Acta.* **173**:427–435.